Reaction Mechanisms

International Edition: DOI: 10.1002/anie.201811454
German Edition: DOI: 10.1002/ange.201811454

Facile Conversion of *syn*-$[Fe^{IV}(O)(TMC)]^{2+}$ into the *anti* Isomer via Meunier's Oxo–Hydroxo Tautomerism Mechanism

Jai Prakash, Yuan Sheng, Apparao Draksharapu, Johannes E. M. N. Klein, Christopher J. Cramer, and Lawrence Que, Jr.**

Abstract: *The syn and anti isomers of $[Fe^{IV}(O)(TMC)]^{2+}$ (TMC = tetramethylcyclam) represent the first isolated pair of synthetic non-heme oxoiron(IV) complexes with identical ligand topology, differing only in the position of the oxo unit bound to the iron center. Both isomers have previously been characterized. Reported here is that the syn isomer $[Fe^{IV}(O_{syn})(TMC)(NCMe)]^{2+}$ (**2**) converts into its anti form $[Fe^{IV}(O_{anti})(TMC)(NCMe)]^{2+}$ (**1**) in MeCN, an isomerization facilitated by water and monitored most readily by ^1H NMR and Raman spectroscopy. Indeed, when $H_2{}^{18}O$ is introduced to **2**, the nascent **1** becomes ^{18}O-labeled. These results provide compelling evidence for a mechanism involving direct binding of a water molecule trans to the oxo atom in **2** with subsequent oxo–hydroxo tautomerism for its incorporation as the oxo atom of **1**. The nonplanar nature of the TMC supporting ligand makes this isomerization an irreversible transformation, unlike for their planar heme counterparts.*

In recent years, polyazamacrocyclic-based and polypyridyl-based ligands have served as surrogates for ligands derived from a protein backbone and contributed significantly to our understanding of metal–oxygen intermediates (M^{n+}–OO^-, M^{n+}–OOH, M^{n+}=O) involved in the catalytic cycles of oxidative enzymatic systems.[1] The ligand topology around the metal center can play an important role in governing the properties of these reactive intermediates.[2] Tetramethylcyclam (TMC)[3] and its derivatives [TMC-L, where one of the four methyl groups in TMC is replaced by an alkyl group bearing a Lewis base that can act as the axial ligand (L) to the metal center] are one such family of ligands for which a variety of iron–oxygen species (such as Fe^{III}–OO^-,[4] Fe^{III}–OOH,[5] Fe^{IV}=O,[6] and Fe^{V}=O[7]) has been characterized by various spectroscopic techniques, as well as X-ray crystallography in a few cases. The common structural features evident in all the crystallographically characterized Fe(TMC) complexes[3,4,6,8] are a) the adoption of the *trans*-I (*R*,*S*,*R*,*S*) configuration[3] with all alkyl groups on one side of the macrocycle and the amine groups forming an equatorial N4 plane around the iron center and b) anionic ligand binding to the iron center almost exclusively *syn* to the methyl groups. An exception to the latter feature is the prototypical oxoiron(IV) complex $[Fe^{IV}(O_{anti})(TMC)(NCMe)](OTf)_2$ (**1**) reported by Rohde et al. in 2003,[6a] the crystal structure of which displays the dianionic oxo ligand bound to the iron center on the *anti* face of the TMC macrocycle. This complex has been extensively characterized with respect to structure and reactivity.[9] Also, crystal structures of related $[Fe^{IV}(O_{anti})(TMC)(OTf)](OTf)$ and $[Fe^{IV}(O_{anti})(TMC)(OH_2)](OTf)_2$ complexes have recently been reported by Schindler and coworkers.[6c] However, the existence of the corresponding *syn* isomer was not unequivocally established until 2015 when the crystal structure of $[Fe^{IV}(O_{syn})(TMC)(OTf)](OTf)$ was described by Prakash et al.[6b] To the best of our knowledge, the two $[Fe^{IV}(O)(TMC)(OTf)]^+$ isomers represent the first pair of crystallographically characterized oxoiron(IV) complexes with the identical ligand topology but with the oxo atom occupying different faces of the TMC macrocycle (Scheme 1). In this work, we focus on the interesting observation that the *syn* isomer converts into its *anti* isomer upon standing. This isomerization is irreversible and is dramatically accelerated by the addition of water. We provide compelling evidence for a proposed mechanism that directly involves a water molecule in this conversion process and is related to the oxo–hydroxo tautomerism mechanism first conceived by Bernadou and

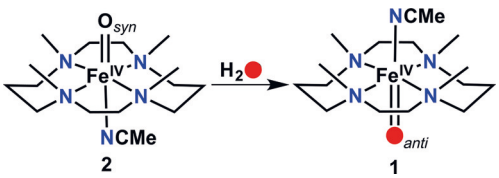

2 1

Scheme 1. Conversion of **2** into **1** facilitated by a water molecule.

[*] Dr. J. Prakash, Y. Sheng, Dr. A. Draksharapu, Dr. J. E. M. N. Klein, Prof. Dr. C. J. Cramer, Prof. Dr. L. Que, Jr.
Department of Chemistry and Center for Metals in Biocatalysis
University of Minnesota
Minneapolis, MN 55455 (USA)
E-mail: larryque@umn.edu
Dr. J. E. M. N. Klein
Molecular Inorganic Chemistry, Stratingh Institute for Chemistry
Faculty of Science and Engineering University of Groningen
Nijenborgh 4, 9747 AG Groningen (The Netherlands)
E-mail: j.e.m.n.klein@rug.nl
Prof. Dr. C. J. Cramer
Chemical Theory Center and Minnesota Supercomputing Institute
University of Minnesota, Minneapolis, MN 55455-0431 (USA)
Dr. J. Prakash
Current address: Department of Physical and Environmental Sciences, Texas A & M University-Corpus Christi
Corpus Christi, TX 78412 (USA)
Supporting information and the ORCID identification number(s) for the author(s) of this article can be found under: https://doi.org/10.1002/anie.201811454.

Meunier for understanding $H_2{}^{18}O$-label exchange in synthetic heme complexes.[10]

The *syn* isomer **2** is generated by adding 1 equivalent of 2-^{t}BuSO$_2$-C$_6$H$_4$IO to an MeCN solution of Fe^{II}(TMC)(OTf)$_2$ at 298 K. The formation of **2** is indicated by a near-IR band at 815 nm ($\varepsilon = 380\,M^{-1}\,cm^{-1}$), and it converts into **1** over 6 h at 298 K with several isosbestic points (see Figure S1 in the Supporting Information). This conversion can also be monitored by ^{1}H NMR spectroscopy, where **2** exhibits a set of seven paramagnetically shifted resonances with a 1:1:2:2:2:2:6 intensity ratio (Figure 1, left; see Figure S2).[6b]

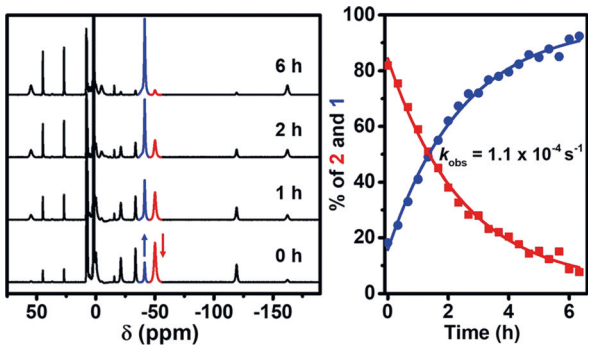

Figure 1. Left: Conversion of 10-mM **2** (*N*-CH$_3$, red) into **1** (*N*-CH$_3$, blue) in CD$_3$CN at 298 K observed by ^{1}H NMR spectroscopy over a 6 h period. Right: Time profile for the intensity changes of the respective *N*-CH$_3$ peaks at −41 and −50 ppm in the conversion of **2** (squares) into **1** (circles) in CD$_3$CN as monitored by ^{1}H NMR spectroscopy at 298 K. Solid lines represent single exponential fits to the experimental data.

There is also a minor amount of **1** present in the solution of **2**, representing about 20% of the Fe in the sample, and it increases over time with a concomitant decrease of **2** such that the starting 4:1 ratio of **2** to **1** becomes 1:10 after 6 hours at 298 K (Figure 1). The growth and the decay of the respective signals of **1** and **2** show exponential behavior, with a first-order rate constant of $1.1 \times 10^{-4}\ s^{-1}$ (Figure 1, right). However, the reverse reaction, that is, the conversion of **1** into **2**, does not occur, suggesting that **2** is the kinetically formed isomer of the thermodynamically favored isomer **1**.

How the conversion of **2** into **1** occurs is an intriguing mechanistic question. One option we considered was that the macrocycle flipped inside out like an umbrella in a windstorm. However, as no isomers other than either **1** or **2** were detected by ^{1}H NMR spectroscopy, such a flip would require simultaneous inversions at all of the TMC N-atoms, an event we deemed implausible. An attractive alternative is for the oxo functionality to relocate from the *syn* position to the *anti* position. The relocation could occur by a mechanism similar to the oxo–hydroxo tautomerism proposed by Bernadou and Meunier (Scheme 2, top)[10] to rationalize the observed exchange of oxo atoms in high-valent heme model complexes with added $H_2{}^{18}O$. In the latter mechanism, binding of the added $H_2{}^{18}O$ to the axial position *trans* to the oxo atom and subsequent loss of a proton from the aqua ligand forms an oxo/hydroxo species, which undergoes facile tautomerization, because of the planarity of the porphyrin ligand, and rapidly

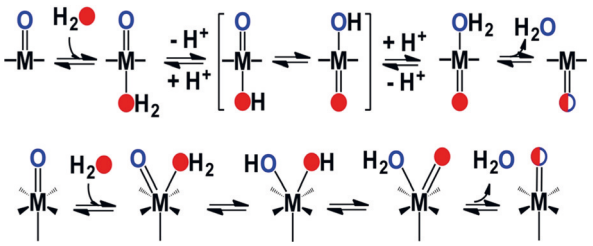

Scheme 2. The oxo–hydroxo tautomerism mechanism proposed by Bernadou and Meunier[10] for O-atom exchange between $H_2{}^{18}O$ and metal-oxo species involving binding of water *trans* to the oxo (top) and the corresponding *cis*-binding variant of Seo et al.[12a] (bottom) Graphic adapted from ref. [12b].

reacts with substrates. Consistent with this scenario, heme oxidation products are generally found to be 50% labelled in the presence of added $H_2{}^{18}O$ (Scheme 2, top), results that suggest the occurrence of only one cycle of ^{18}O-label exchange.[11]

The conversion of **2** into **1** must follow a mechanism somewhat different from the above scenario, as TMC is a nonplanar ligand. Thus **1** and **2** are not equivalent and the conversion of **2** into **1** might then be expected to be irreversible with full incorporation of the $H_2{}^{18}O$-derived O-atom into **1** (Scheme 3). Our NMR studies of **1** in aqueous solution show that **1** is an oxo-aqua species with no evidence for the oxo-hydroxo conjugate base, which forms under more basic conditions and exhibits a clearly distinct NMR spectral pattern.[13] Thus, tautomerization is proposed to occur via a *trans*-dihydroxoiron(IV) species.

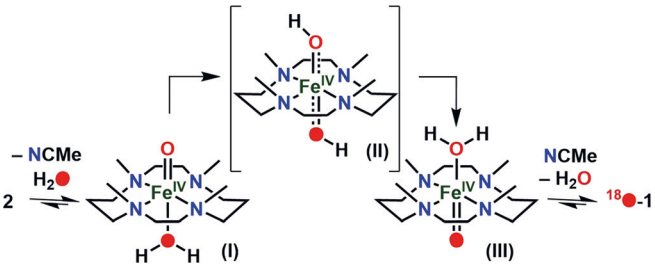

Scheme 3. Modified mechanism proposed for the conversion of **2** into **1**.

To test this idea, we monitored the conversion of **2** into **1** in the presence of added water. A 10 mM solution of **2** in CD$_3$CN containing 0.1M H_2O was monitored by ^{1}H NMR spectroscopy, and **2** converted into **1** at 298 K within 1400 s ($k_{obs} = 2.0 \times 10^{-3}\ s^{-1}$; Figure 2 A), a 20-fold rate acceleration relative to the reaction in pure CD$_3$CN ($k_{obs} = 1.1 \times 10^{-4}\ s^{-1}$, Figure 1). Monitoring this conversion by Raman spectroscopy under the same conditions, except for the use of $H_2{}^{18}O$ (Figure 2 B), shows that the 858 cm^{-1} peak associated with ν(Fe=O) of ^{16}O-**2** decays over time with concomitant formation of a new peak at 804 cm^{-1}, corresponding to the ν(Fe=O) of [^{18}O]**1**. These changes occur at a rate (Figure 2 C) comparable to that deduced from the NMR data in Figure 2 A. That the peak at 804 cm^{-1} grows over time at the

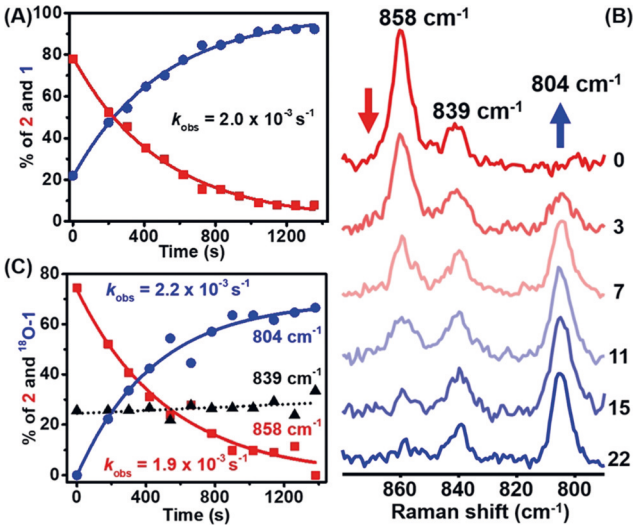

Figure 2. A) Plot of intensity changes for the *N*-Me protons observed by ^{1}H NMR spectroscopy versus time in the conversion of **2** (squares) into **1** (circles) (10 mM **2** in CD_3CN with 0.10 M H_2O at 298 K). B) Raman spectral changes observed for a 10 mM solution of **2** (generated in MeCN with 1 equiv 2-^{t}BuSO_2-C_6H_4IO added as a solid) containing 0.10 M $H_2{}^{18}O$ over a period of 22 min at 298 K. Numbers to the right of each spectrum indicate how many minutes after sample preparation the spectra were collected. The peaks at 858, 839, and 804 cm^{-1} are associated with ν(Fe=O)'s of [^{16}O]**2**, [^{16}O]**1**, and [^{18}O]**1**, respectively. No peak corresponding to [^{18}O]**2** (820 cm^{-1}) was observed. C) Time profile for the decay of the 858 cm^{-1} peak (squares) and the growth of the 804 cm^{-1} peak (circles). No significant change was observed in the intensity of the 839 cm^{-1} peak (triangles). Lines represent single exponential fits to the data.

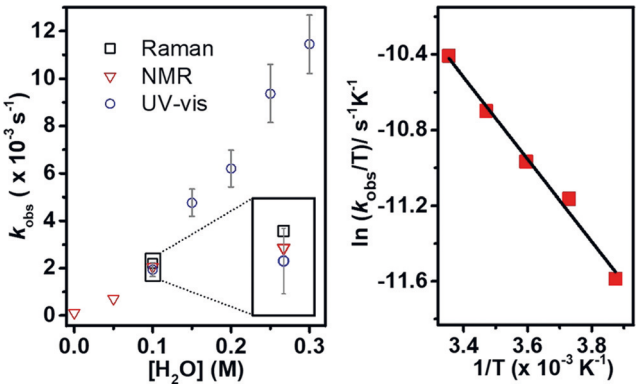

Figure 3. Left: Plot of first-order rate constants for the conversion of **2** into **1** in MeCN at 298 K by following changes in the UV-vis absorption and the NMR and Raman spectra versus concentration of the added water (see Table S1). Right: Eyring plot for the conversion of **2** into **1** in MeCN between 258 and 298 K in the presence of 0.25 M H_2O.

expense of the peak at 858 cm^{-1} (Figure 2 B) provides direct evidence for $H_2{}^{18}O$ binding to **2** and subsequent incorporation of the O atom from $H_2{}^{18}O$ as the oxo atom of **1**. That the peak corresponding to [^{18}O]**2** (expected at 820 cm^{-1} based on Hooke's law)[6b] is not observed in the Raman experiment rules out the corresponding *cis*-binding mechanism as proposed by Seo et al.[11a] (Scheme 2, bottom) for ^{18}O incorporation from $H_2{}^{18}O$ into **1** in a label-exchange reaction. Instead, our data fit well with the mechanism shown in Scheme 3 where $H_2{}^{18}O$ binds the iron center *trans* to the oxo moiety of **2** (species **I**), undergoes tautomerization to form a transient *trans*-Fe^{IV}(^{16}OH)(^{18}OH) species (**II**), and eventually yields Fe^{IV}(^{18}O) with the exchanged ^{18}O atom occupying the position *trans* to the initial oxo moiety (species **III**). The original oxo atom becomes a water molecule at the end of the reaction and is displaced by the MeCN solvent. Of note is the relative invariance in the intensity of the peak at 839 cm^{-1}, which derives from [^{16}O]**1** that is observed from the start, showing that this minor component of the reaction mixture is not involved in the ^{18}O-exchange process under these conditions.

Additional experiments following changes in the UV-vis-NIR absorption, NMR, and Raman spectra show that the rate of conversion from **2** into **1** is accelerated with an increase in the concentration of the added water (Figure 3, left; see Table S1). A linear fit of the accumulated data gives a second rate constant of 3.5×10^{-2} M^{-1} s^{-1}, supporting the involvement of a water molecule in the conversion. In contrast, a study starting with different amounts of **2** in the presence of 0.1 M H_2O shows the conversion to be independent of [**2**] (see Table S1). Interestingly, when 0.1 M D_2O is added instead of H_2O, a KIE of 2 is observed (see Figure S3), implicating a role for the subsequent proton transfer events in the conversion. An Eyring analysis of the temperature dependence of the rate constants between 258 and 298 K by following spectral changes in the near IR region in MeCN solutions containing 0.25 M H_2O affords activation parameters of $\Delta H^{\ddagger} =$ 18(2) kJ mol^{-1} and $\Delta S^{\ddagger} = -225(20)$ J mol^{-1} K^{-1} (Figure 3, right) for the conversion of **2** into **1**. The large and negative value of $\Delta S^{\ddagger}$ demonstrates the key role of a water molecule in effecting this conversion, consistent with the mechanism shown in Scheme 3. Interestingly, the above results resemble those reported for $H_2{}^{18}O$ exchange into the Fe=O unit of **1** under comparable conditions,[12b] suggesting closely related mechanisms that differ only in having a *trans*- or a *cis*-dihydroxoiron(IV) intermediate (Scheme 2).[14]

We have also probed whether the pathway shown in Scheme 3 is energetically viable using computational methods. For this purpose, all structures have been optimized at the TPSS-D3(BJ)/def2-TZVP level of theory in the gas phase[15] and are depicted in Figure 4. The calculated structural parameters agree with those established by crystallography (see Table S2).[6] We note here that two conformations of the TMC ligand have been considered, where the ethylene linkages are oriented in either a crossed or parallel conformation (see Figures S4 and S6). We only show the parallel conformation in Figure 4 for simplicity and provide energetic values for the crossed conformation in square brackets.

To obtain accurate energies, we computed the free energies of solvation with the SMD solvation model[16] to simulate MeCN solvation for the gas-phase structures. To improve the accuracy of the electronic energies we recomputed them using the random phase approximation (RPA)[17] in a post Kohn–Sham fashion (i.e., using the TPSS KS orbitals; RPA@TPSS) with the def2-QZVPP basis set.[14d] For a detailed description and justification of the computational procedure, see the Supporting Information.

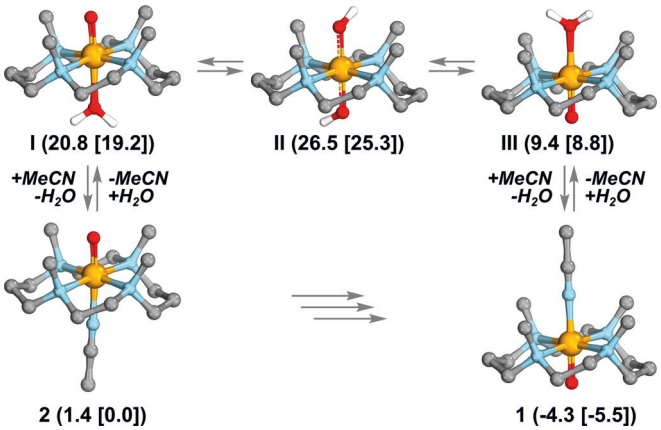

Figure 4. Structural depictions and relative energetics (ΔG_{298K} in kJ mol^{-1}) for the proposed H_2O-assisted interconversion of **2** into **1**. H atoms of the TMC ligand are not depicted for clarity and only the parallel conformation is shown. Energies for the crossed conformation are provided in brackets. Free energies are reported at the RPA@TPSS/def2-QZVPP//TPSS-D3(BJ)/def2-TZVP level of theory in the gas phase and include free energy of solvation at the TPSS-D3(BJ)/def2-TZVP/SMD(MeCN) level of theory. Structural depictions were made using IboView.[18]

At this correlated wavefunction level of theory, we indeed find that the *anti* isomer **1** is energetically the lowest in energy and thus thermodynamically favored. More importantly, the primary conclusion to be drawn from the calculations is that **I**, **II**, and **III** are clearly energetically accessible intermediates at room temperature for the isomerization from **2** into **1**. Although we have not attempted to follow the specific series of deprotonations and reprotonations (or extended proton shuttling events) necessary to interconvert the tautomers of the H_2O-bound intermediates, such proton transfers generally are facile in polar solvents. One additional feature to consider is the varying concentrations of MeCN and H_2O, as the outlined process involves the loss/gain of a solvent molecule. In the energetics in Figure 4 we have not taken this into account, as this will strictly depend on the ratio of MeCN to H_2O. We note, however, that with an increasing H_2O concentration and a decreasing MeCN concentration **I**, **II**, and **III** become energetically more favorable by several kJ mol^{-1}.[19]

In conclusion, the conversion of the *syn* isomer **2** into its *anti* form **1** in the presence of added water has been investigated by UV-vis absorption, Raman, and ^{1}H NMR spectroscopy. Addition of water clearly accelerates this transformation, and the rate of conversion has a first-order dependence on water concentration (Figure 3, left panel). Importantly, the O-atom from a water molecule is incorporated as the oxo atom of **1** based on Raman experiments using $H_2{}^{18}O$ (Figure 2B). Eyring analysis of the conversion of **2** into **1** reveals a large and negative $\Delta S^{\ddagger}$, supporting water binding to **2** at or before the rate-determining step. Water binding to **2** may be facilitated by dissociation of the weakly bound axial ligand of **2**, which has been shown to have an Fe–O_{axial} bond of 2.15 Å in the crystal structure of $[Fe^{IV}(O_{syn})(TMC)(OTf)]^+$.[6b] This distance is 0.1 Å longer than corresponding bonds in the *anti* complexes.[6a,c] Subsequent to binding H_2O *trans* to the oxo atom of **2** (**I** in Scheme 3), oxo-aqua tautomerism occurs to form a *trans*-dihydroxoiron(IV) intermediate (**II** in Scheme 3), which in turn converts into **1**. The mechanism in Scheme 3 is a slight variation of the Meunier mechanism for synthetic heme complexes,[10] and explains the 50% incorporation of $H_2{}^{18}O$ label into the oxidation products resulting from the plano-symmetric nature of the metalloporphyrin moiety.[11] Instead, quantitative and irreversible ^{18}O labeling of **1** from $H_2{}^{18}O$ is observed in the conversion of the non-plano-symmetric **2** into its thermodynamically favored isomer **1** (Scheme 3). Tetramethylcyclam is thus unique among tetradentate ligands with all four donors occupying the equatorial plane and giving rise to two distinct Fe^{IV}=O isomers that have distinct topologies relative to the ferryl moiety.

Experimental Section

For details of the synthetic procedures and the physical and experimental methods, see the Supporting Information. **Caution:** 2-^{t}BuSO$_2$-C$_6$H$_4$IO was used as a reagent for this work. Its synthesis recently led to an injury of a researcher. Appropriate safety measures should be taken.[20]

Acknowledgements

This work was supported by a grant from the U.S. National Science Foundation (CHE-1665391 to L.Q. and CHE-1361595 to C.J.C.). J.E.M.N.K. thanks the Alexander von Humboldt Foundation for a Feodor Lynen Research Fellowship. The authors acknowledge the Minnesota Supercomputing Institute (MSI) at the University of Minnesota for providing resources that contributed to the research results reported within this paper. We would also like to thank the Center for Information Technology of the University of Groningen for their support and for providing access to the Peregrine high-performance computing cluster.

Conflict of interest

The authors declare no conflict of interest.

Keywords: isomers · iron · macrocycles · reaction mechanisms · tautomerism

How to cite: *Angew. Chem. Int. Ed.* **2019**, *58*, 1995–1999
Angew. Chem. **2019**, *131*, 2017–2021

[1] a) A. R. McDonald, L. Que, Jr., *Coord. Chem. Rev.* **2013**, *257*, 414–428; b) W. Nam, *Acc. Chem. Res.* **2015**, *48*, 2415–2423; c) J. E. M. N. Klein, L. Que, Jr. in *Encyclopedia of Inorganic and Bioinorganic Chemistry*, Wiley, Hoboken, **2016**, https://doi.org/10.1002/9781119951438.eibc9781119952344.

[2] a) D. Wang, K. Ray, M. J. Collins, E. R. Farquhar, J. R. Frisch, L. Gomez, T. A. Jackson, M. Kerscher, A. Waleska, P. Comba, M. Costas, L. Que, Jr., *Chem. Sci.* **2013**, *4*, 282–291; b) S. Hong, Y.-M. Lee, K.-B. Cho, K. Sundaravel, J. Cho, M. J. Kim, W. Shin, W. Nam, *J. Am. Chem. Soc.* **2011**, *133*, 11876–11879; c) J. England,

J. Prakash, M. A. Cranswick, D. Mandal, Y. Guo, E. Münck, S. Shaik, L. Que, Jr., *Inorg. Chem.* **2015**, *54*, 7828 – 7839.
[3] a) E. K. Barefield, *Coord. Chem. Rev.* **2010**, *254*, 1607 – 1627; b) S. P. de Visser, J.-U. Rohde, Y.-M. Lee, J. Cho, W. Nam, *Coord. Chem. Rev.* **2013**, *257*, 381 – 393.
[4] J. Cho, S. Jeon, S. A. Wilson, L. V. Liu, E. A. Kang, J. J. Braymer, M. H. Lim, B. Hedman, K. O. Hodgson, J. S. Valentine, E. I. Solomon, W. Nam, *Nature* **2011**, *478*, 502 – 505.
[5] F. Li, K. K. Meier, M. A. Cranswick, M. Chakrabarti, K. M. Van Heuvelen, E. Münck, L. Que, Jr., *J. Am. Chem. Soc.* **2011**, *133*, 7256 – 7259.
[6] a) J.-U. Rohde, J.-H. In, M. H. Lim, W. W. Brennessel, M. R. Bukowski, A. Stubna, E. Münck, W. Nam, L. Que, Jr., *Science* **2003**, *299*, 1037 – 1039; b) J. Prakash, G. T. Rohde, K. K. Meier, E. Münck, L. Que, Jr., *Inorg. Chem.* **2015**, *54*, 11055 – 11057; c) S. Schaub, A. Miska, J. Becker, S. Zahn, D. Mollenhauer, S. Sakshath, V. Schuenemann, S. Schindler, *Angew. Chem. Int. Ed.* **2018**, *57*, 5355 – 5358; *Angew. Chem.* **2018**, *130*, 5453 – 5456.
[7] K. M. Van Heuvelen, A. T. Fiedler, X. Shan, R. F. De Hont, K. K. Meier, E. L. Bominaar, E. Münck, L. Que, Jr., *Proc. Natl. Acad. Sci. USA* **2012**, 11933 – 11938.
[8] a) J. England, J. O. Bigelow, K. M. Van Heuvelen, E. R. Farquhar, M. Martinho, K. K. Meier, J. R. Frisch, E. Münck, L. Que, *Chem. Sci.* **2014**, *5*, 1204 – 1215; b) A. R. McDonald, M. R. Bukowski, E. R. Farquhar, T. A. Jackson, K. D. Koehntop, M. S. Seo, R. F. De Hont, A. Stubna, J. A. Halfen, E. Münck, W. Nam, L. Que, Jr., *J. Am. Chem. Soc.* **2010**, *132*, 17118 – 17129; c) K. D. Hodges, R. G. Wollmann, S. L. Kessel, D. N. Hendrickson, D. G. Van Derveer, E. K. Barefield, *J. Am. Chem. Soc.* **1979**, *101*, 906 – 917.
[9] a) C. V. Sastri, J. Lee, K. Oh, Y. J. Lee, J. Lee, T. A. Jackson, K. Ray, H. Hirao, W. Shin, J. A. Halfen, J. Kim, L. Que, Jr., S. Shaik, W. Nam, *Proc. Natl. Acad. Sci. USA* **2007**, *104*, 19181 – 19186; b) T. A. Jackson, J.-U. Rohde, M. S. Seo, C. V. Sastri, R. DeHont, A. Stubna, T. Ohta, T. Kitagawa, E. Münck, W. Nam, L. Que, Jr., *J. Am. Chem. Soc.* **2008**, *130*, 12394 – 12407; c) S. Fukuzumi, Y. Morimoto, H. Kotani, P. Naumov, Y.-M. Lee, W. Nam, *Nat. Chem.* **2010**, *2*, 756 – 759.
[10] J. Bernadou, B. Meunier, *Chem. Commun.* **1998**, 2167 – 2173.
[11] a) J. Bernadou, A.-S. Fabiano, A. Robert, B. Meunier, *J. Am. Chem. Soc.* **1994**, *116*, 9375 – 9376; b) M. Pitié, J. Bemadou, B. Meunier, *J. Am. Chem. Soc.* **1995**, *117*, 2935 – 2936; c) R. J. Balahura, A. Sorokin, J. Bernadou, B. Meunier, *Inorg. Chem.* **1997**, *36*, 3488 – 3492; d) K. A. Lee, W. Nam, *J. Am. Chem. Soc.* **1997**, *119*, 1916 – 1922; e) S. J. Yang, W. Nam, *Inorg. Chem.* **1998**, *37*, 606 – 607; f) N. Jin, J. L. Bourassa, S. C. Tizio, J. T. Groves, *Angew. Chem. Int. Ed.* **2000**, *39*, 3849 – 3851; *Angew. Chem.* **2000**, *112*, 4007 – 4009.
[12] a) M. S. Seo, J.-H. In, S. O. Kim, N. Y. Oh, J. Hong, J. Kim, L. Que, Jr., W. Nam, *Angew. Chem. Int. Ed.* **2004**, *43*, 2417 – 2420; *Angew. Chem.* **2004**, *116*, 2471 – 2474; b) M. Puri, A. Company, G. Sabenya, M. Costas, L. Que, *Inorg. Chem.* **2016**, *55*, 5818 – 5827.
[13] J. E. M. N. Klein, A. Draksharapu, A. Shokri, C. J. Cramer, L. Que, Jr., *Chem. Eur. J.* **2018**, *24*, 5373 – 5378.
[14] An alternative mechanism for water-label incorporation into **1** has been suggested in Ref. [12b] and involves two cycles of water exchange, with labeled water binding *trans* to the oxo of **1** followed by tautomerization to form oxo-labeled **2** in the first cycle, and then a second axial ligand exchange to introduce labeled water *trans* to the oxo of **2** followed by tautomerization to form oxo-labeled **1** in the next cycle. This scenario would entail only fleeting involvement of the kinetic product **2**.
[15] a) J. Tao, J. P. Perdew, V. N. Staroverov, G. E. Scuseria, *Phys. Rev. Lett.* **2003**, *91*, 146401; b) S. Grimme, J. Antony, S. Ehrlich, H. Krieg, *J. Chem. Phys.* **2010**, *132*, 154104; c) S. Grimme, S. Ehrlich, L. Goerigk, *J. Comput. Chem.* **2011**, *32*, 1456 – 1465; d) F. Weigend, R. Ahlrichs, *Phys. Chem. Chem. Phys.* **2005**, *7*, 3297 – 3305.
[16] A. V. Marenich, C. J. Cramer, D. G. Truhlar, *J. Phys. Chem. B* **2009**, *113*, 6378 – 6396.
[17] G. P. Chen, V. K. Voora, M. M. Agee, S. G. Balasubramani, F. Furche, *Annu. Rev. Phys. Chem.* **2017**, *68*, 421 – 445.
[18] a) G. Knizia, J. E. M. N. Klein, *Angew. Chem. Int. Ed.* **2015**, *54*, 5518 – 5522; *Angew. Chem.* **2015**, *127*, 5609 – 5613; b) G. Knizia, http://www.iboview.org/.
[19] For a reference disussing this aspect, see: V. S. Bryantsev, M. S. Diallo, W. A. Goddard III, *J. Phys. Chem. B* **2008**, *112*, 9709 – 9719.
[20] "Chemical Safety: Synthesis Procedure": J. T. Hupp, S. T. Nguyen, *Chem. Eng. News* **2011**, *89*, 2.

Manuscript received: October 5, 2018
Revised manuscript received: November 27, 2018
Accepted manuscript online: December 16, 2018
Version of record online: January 17, 2019

